Advances in Science and Technology Research Journal

Advances in Science and Technology Research Journal, 2026, 20(5), 360–371
https://doi.org/10.12913/22998624/216388
ISSN 2299-8624, License CC-BY 4.0

Received: 2025.10.05
Accepted: 2026.03.15
Published: 2026.04.01

Influence of artificial aging temperature on the T6-treated vertical centrifugal casting of re-melted pistons reinforced with copper and silica sand

Teguh Triyono[1], Raihan Aulia Rahman[1], Eko Surojo[1], Aditya Rio Prabowo[1], Triyono[1*]

[1] Mechanical Engineering Department, Universitas Sebelas Maret, Surakarta, Indonesia
* Corresponding author's email: triyono74@staff.uns.ac.id

ABSTRACT

This study utilized recycled aluminum derived from used pistons reinforced with copper (Cu) and silica sand (SiO_2) to produce an aluminum matrix composite (AMC). Fabrication was carried out using the vertical centrifugal casting method, resulting in a radial microstructural gradient characteristic of functionally graded materials (FGMs). The cast products were subsequently subjected to T6 heat treatment, consisting of solution treatment at 505 °C for 5 h, quenching in water, followed by artificial aging at varied temperatures of 140 °C, 170 °C, and 200 °C for 7 h. Characterization involved microstructural observation, Brinell hardness testing, and impact strength evaluation. Microstructural analysis revealed that aging at 170 °C generated fine, uniformly distributed Al_2Cu precipitates, yielding the highest hardness of 138.96 BHN in the outer region. In contrast, aging at 200 °C led to precipitate coarsening and marked spheroidization of β-Si, resulting in reduced hardness but the highest impact toughness, reaching 4.71 J in the inner region. These findings demonstrate a clear trade-off between hardness and toughness, highlighting that peak-aged conditions (170 °C) maximize strength, whereas over-aged conditions (200 °C) enhance fracture resistance. Overall, the combination of recycling, particle reinforcement, and optimized heat treatment provides a viable pathway for producing high-performance aluminum composites for engineering applications.

Keywords: recycled aluminum, aluminum matrix composite, vertical centrifugal casting, artificial aging, toughness.

INTRODUCTION

Aluminum is a lightweight non-ferrous metal widely utilized in automotive and aerospace industries due to its high specific strength, good wear resistance, and excellent corrosion resistance [1]. However, the extraction of primary aluminum from bauxite ore is highly energy-intensive and raises significant environmental concerns [2]. Recycling aluminum through re-melting offers a more sustainable and cost-effective alternative, yet its repeated cycles often lead to a decline in hardness and strength [3–5]. Alloying additions, particularly copper (Cu), have been shown to restore and improve properties by forming intermetallic phases such as Al_2Cu, which contribute to precipitation hardening and improved thermal stability [6,7]. In parallel, Al-Si alloys are known for their high strength and castability, but they are often prone to solidification defects such as hot tearing, underscoring the need for advanced processing strategies to optimize their performance [8].

To address these challenges, aluminum matrix composites (AMCs) have emerged as a promising solution [9]. Reinforcing aluminum with ceramic particles, such as SiC, Al_2O_3, or SiO_2, has proven effective in improving hardness, wear resistance, and tensile strength [10]. Among various methods for fabricating AMCs, centrifugal casting is advantageous because it enhances particle distribution and minimizes porosity. In particular, vertical centrifugal casting utilizes centrifugal force to redistribute phases and reinforcements according to density differences. This naturally produces a

functionally graded material (FGM) structure, where harder, denser constituents concentrate near the outer surface while the inner region retains toughness [11,12]. Such a microstructural gradient is beneficial for applications requiring simultaneous resistance to wear and impact. Incorporating SiO_2 as reinforcement in re-melted aluminum alloys aligns with this approach, offering both property enhancement and sustainability through the utilization of abundant silica resources [13].

Beyond fabrication, post-casting heat treatment plays a critical role in optimizing the performance of aluminum alloys and composites. The T6 treatment, consisting of solution treatment followed by artificial aging, is widely applied to induce precipitation hardening [14,15]. During artificial aging, controlled diffusion promotes the nucleation and growth of precipitates such as Al_2Cu, which obstruct dislocation motion and increase hardness [16]. The effectiveness of this process depends strongly on the aging temperature: under-aging results in incomplete precipitation, whereas over-aging leads to precipitate coarsening, reducing hardness while sometimes improving toughness. Previous studies have reported peak hardness in Al-Cu-based alloys at aging temperatures around 170–175 °C, while higher temperatures accelerate over-aging and property degradation [17–19]. However, most of this research has been conducted on conventional cast or wrought alloys, with limited attention to materials produced by centrifugal casting, where a graded microstructure can alter the precipitation response in different regions.

Despite existing research on recycled aluminum, heat treatment, and composite strengthening, studies clarifying how artificial aging temperature affects precipitation behavior, microstructural gradient, and mechanical properties in remelted aluminum alloys strengthened simultaneously with Cu and SiO_2 under vertical centrifugal casting are still limited. This work addresses this gap by examining the effect of aging temperature on the microstructural evolution and mechanical performance of remelted aluminum piston alloys processed via vertical centrifugal casting. The interaction between centrifugal force-induced microstructural gradient and T6 precipitation behavior has not been systematically evaluated in previous studies. The findings of this work provide new insights into how graded microstructures respond to precipitation mechanisms during T6 treatment, thus offering a more complete picture of recycled aluminum matrix composites produced via centrifugal casting.

EXPERIMENTAL METHOD

Recycled aluminum from used pistons was used as the base material, reinforced with 3 wt.% copper (Cu) and 3 wt.% silica (SiO_2). The silica sand and copper used were in powder form, sieved to a 200-mesh sieve with a size of approximately 0.075 mm. Copper and silica reinforcements were used in the form of commercially available powders. The Cu powder exhibited an irregular/angular morphology typically produced through gas atomization or mechanical milling. Meanwhile, the SiO_2 powder showed an angular–irregular shape characteristic of silica powders obtained by quartz grinding. Both powders were supplied in dry powder form without additional surface treatment.

The results of testing chemical compositions of the re-melted piston alloy is shown in Table 1. The aluminum scrap was melted in a crucible furnace at 850 °C, while the permanent steel mold was preheated to 500 °C. After the melt reached the target temperature, Cu and SiO_2 particles were introduced and stirred at 400 rpm for 4 minutes to improve particle dispersion. The molten composite was then poured into a vertical centrifugal casting mold rotating at 1000 rpm for 3 minutes, producing a cylindrical specimen with a radial gradient structure due to centrifugal force. The permanent mold and specimen geometry are presented in Figure 1. The samples used for testing were cut crosswise and then analyzed based on three main zones: outer, middle, and inner (Figure 2).

Table 1. Chemical composition of the re-melted piston alloy (wt.%)

Element	%wt
Si	11.28
Fe	1.412
Cu	0.956
Mn	0.162
Mg	1.034
Cr	0.034
Ni	1.061
Zn	0.239
Ti	0.028
Pb	0.011
Al	83.75

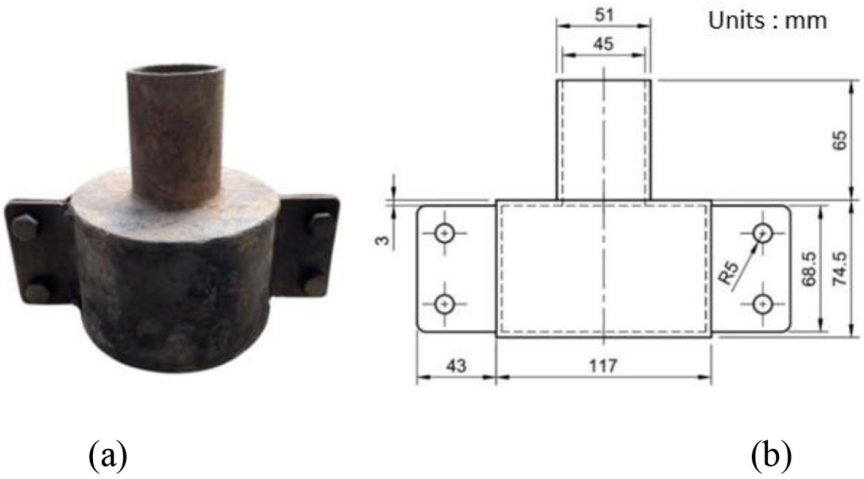

Figure 1. (a) Permanent mold, (b) Geometry of the permanent mold

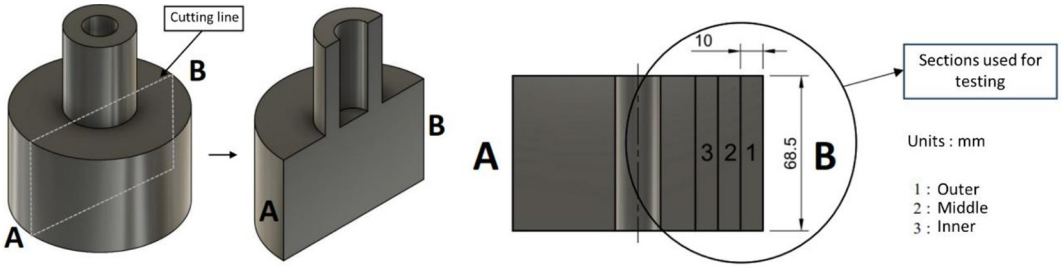

Figure 2. Cast specimen cutting and specimen characteristic testing scheme

The as-cast specimens underwent T6 heat treatment, which consisted of solution treatment at 505 °C for 5 h, quenching in water at room temperature, and artificial aging at three different temperatures: 140 °C, 170 °C, and 200 °C, each for 7 h. This sequence was designed to evaluate the influence of aging temperature on microstructural development and mechanical performance of the composite material.

Microstructural characterization was performed using optical microscopy after standard metallographic preparation and etching with Keller's reagent (ASTM E407-07) to examine the distribution of SiO_2 and Cu particles within the matrix. Brinell hardness testing was carried out in accordance with ASTM E10 using tungsten carbide ball indenters under loads of 9806,65 N, with dwell times of 10 s. Hardness measurements were taken at different radial regions to account for the functionally graded nature of the material. Charpy impact tests were conducted in accordance with ASTM E23 using V-notched specimens, with specimen dimensions shown in Figure 3. The impact test was carried out at room temperature.

RESULTS AND DISCUSSION

XRD results

XRD analysis of SiO_2 powder shows a dominant quartz phase ($SiO_2 \approx 67.6\%$) with the presence of minor oxides such as Al_2O_3, Fe_2O_3, TiO_2, and CaO. SiO_2 particles are hard, inert, and stable at aluminum casting temperatures (Table 2). The detected Al_2O_3 and Fe_2O_3 contents indicate that the silica powder is not pure silica but rather naturally derived silica, which is commonly found in mineral milling materials. The presence of these minor phases may affect the wetting behavior of the Al matrix during mixing. Although the XRD analysis was performed on SiO_2 powder, the results provide an important context for understanding the microstructural evolution of the composite during vertical centrifugal casting and T6 treatment. The SEM morphology of SiO_2 on aluminum can be seen in Figure 4. From this figure, it can be seen that SiO_2 is identified as dark in color, which is proven by the EDS results which show the dominant elements Si and O.

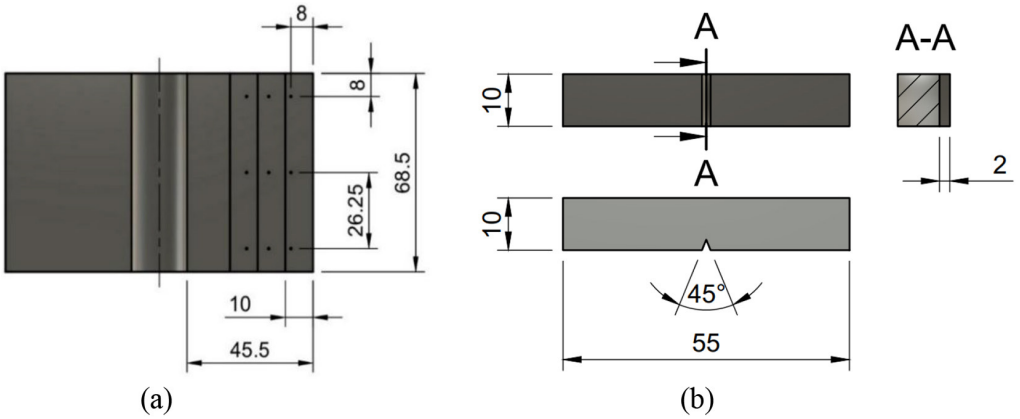

Figure 3. Dimensions of test specimens: (a) Brinell hardness specimen and (b) Charpy impact specimen

Table 2. XRD results of SiO_2

No.	Component	Result	Unit	El. line	Intensity	Analyzing depth
1.	Total	13.30	mg/cm^2			
2.	AL_2O_3	2.40	Mass %	Al-KA	1.5244	0.0101
3.	SiO_2	67.6	Mass %	Si-KA	43.0445	0.0139
4.	SO_3	0.0443	Mass %	S-KA	0.0459	0.0151
5.	Cl	0.0118	Mass %	Cl-KA	0.0480	0.0199
6.	K_2O	0.211	Mass %	K-KA	0.3521	0.0453
7.	CaO	0.151	Mass %	Ca-KA	0.3994	0.0604
8.	TiO_2	0.108	Mass %	Ti-KA	0.0693	0.1012
9.	Fe_2O_3	0.216	Mass %	Fe-KA	1.0291	0.2739
10.	NiO	0.0096	Mass %	Ni-KA	0.0989	0.4270
11.	Balance	29.3	Mass %	Pd-KAC	10.6277	

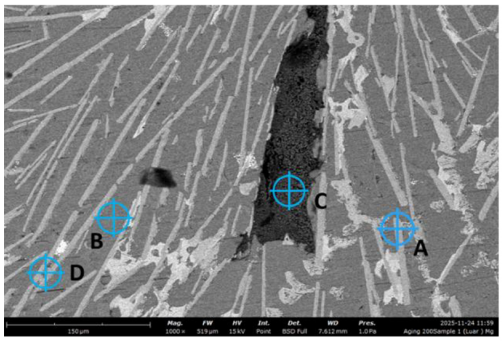

	Element Number	Element Symbol	Element Name	Atomic Conc.	Weight Conc.
A	8	O	Oxygen	0.390	0.200
	11	Na	Sodium	0.000	0.000
	13	Al	Aluminum	72.383	62.663
	14	Si	Silicon	13.100	11.812
	17	Cl	Chlorine	0.000	0.000
	26	Fe	Iron	14.127	25.325
B	8	O	Oxygen	0.841	0.500
	11	Na	Sodium	0.351	0.300
	13	Al	Aluminum	97.724	97.900
	14	Si	Silicon	0.863	0.900
	17	Cl	Chlorine	0.076	0.100
	26	Fe	Iron	0.145	0.300
C	8	O	Oxygen	52.405	39.640
	11	Na	Sodium	0.184	0.200
	12	Mg	Magnesium	15.758	18.118
	13	Al	Aluminum	7.301	9.309
	14	Si	Silicon	24.046	31.932
	17	Cl	Chlorine	0.060	0.100
	26	Fe	Iron	0.190	0.501
	33	As	Arsenic	0.057	0.200
D	8	O	Oxygen	0.493	0.200
	11	Na	Sodium	0.000	0.000
	13	Al	Aluminum	62.647	42.757
	14	Si	Silicon	0.562	0.400
	17	Cl	Chlorine	0.111	0.100
	26	Fe	Iron	0.212	0.300
	28	Ni	Nickel	13.049	19.381
	29	Cu	Copper	22.925	36.863

Figure 4. SEM morphology of SiO_2

METALLOGRAPHY OBSERVATION

The microstructural investigations showed that the cooling rate and centrifugal forces were the main factors influencing the phase distribution in the outer, middle, and inner segments of the vertical centrifugal casting. Figure 5 illustrates that the dominant matrix in all regions was α-Al, accompanied by secondary phases such as eutectic β-Si, Al_2Cu precipitates, SiO_2 reinforcement particles, and β-Al_5FeSi intermetallics. The morphology, size, and spatial distribution of these phases vary significantly between segments and strongly influence the resulting mechanical properties.

Based on their low density and centrifugal segregation, the inner segment's slower cooling produced concentrated SiO_2 particles and coarse dendritic grains, whereas the outer segment's quick cooling created fine equiaxed α-Al grains and uniform phase dispersion. A comparatively balanced phase distribution and intermediate particle sizes were seen in the middle segment.

The artificial aging temperature had a critical role in modifying the morphology and stability of strengthening phases. At 140 °C, the material remained under-aged, with β-Si retained in its acicular form and Al_2Cu precipitates still limited to early GP zones, leading to insufficient strengthening. Zamani et al said that keeping aging temperature in the low part of the interval (e.g., ≲ 160 °C) slows solute diffusion and delays the formation of equilibrium Al_2Cu [19]. At an aging temperature of around 170 °C, the microstructure exhibited more favorable characteristics. The eutectic β-Si particles transformed into a more globular (spheroidized) morphology, while fine and uniformly distributed Al_2Cu precipitates formed at the early strengthening stages. These features effectively hindered dislocation motion and enhanced grain boundary stability, particularly in the outer regions where significant grain

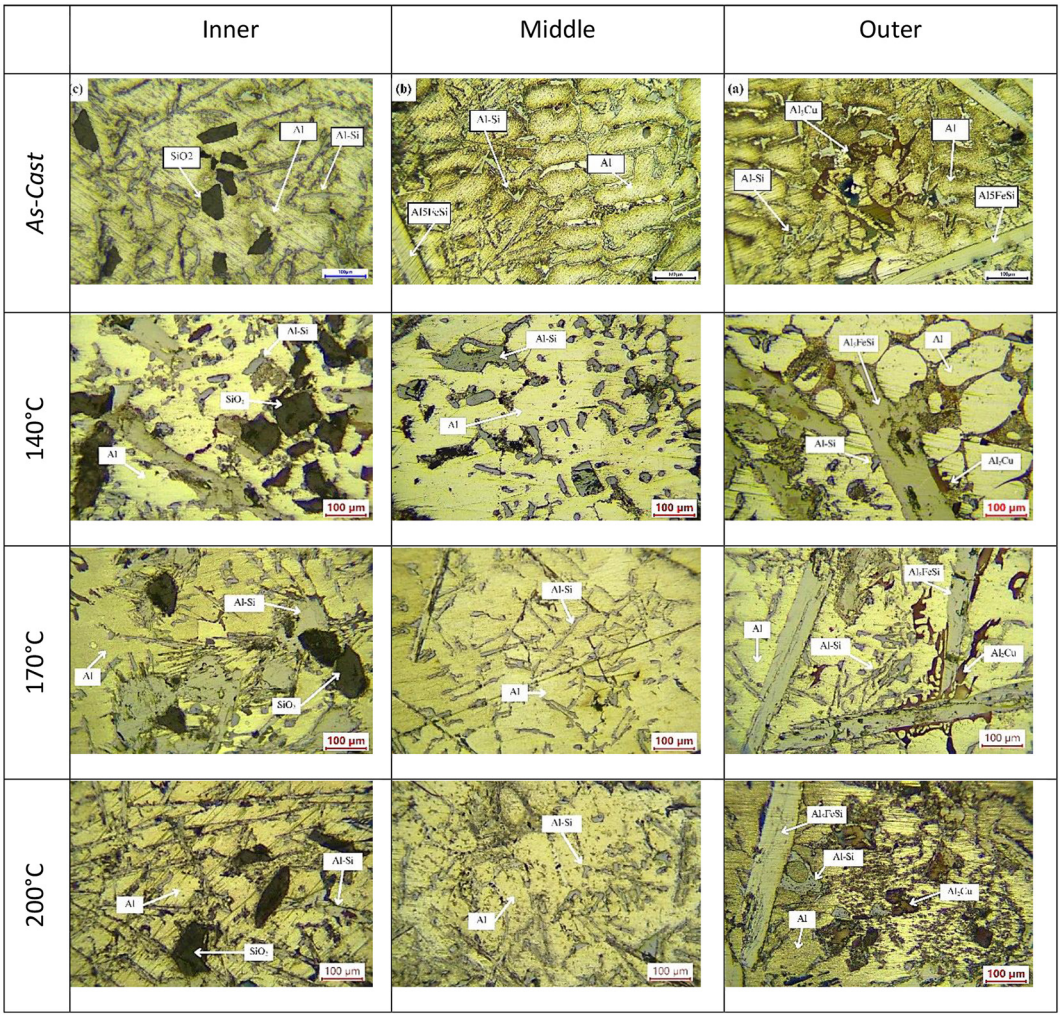

Figure 5. Microstruture of inner, middle and outer segment of composites with artificial aging treatment

refinement had already occurred due to rapid solidification. In contrast, when the temperature was increased to about 200 °C, over-aging took place, characterized by the coarsening of Al_2Cu precipitates and the regrowth or coarsening of Si particles, which reduced the efficiency of precipitation hardening. Nevertheless, β-Si spheroidization was more advanced at this temperature, especially in the inner segment, which enhanced resistance to crack initiation despite the coarser grain structure [20–22].

HARDNESS DISTRIBUTION

The Brinell hardness measurements shown in Figure 6 strongly support the microstructural data obtained through metallography. A clear radial gradient in hardness was observed, with the outer segment consistently exhibiting the highest values, followed by the middle and inner segments. The highest hardness measured in this study 138.96 BHN occurred in the outer region at the artificial aging temperature of 170 °C, confirming this as the peak-aged condition.

The outer segment's greater hardness is directly due to its refined microstructural characteristics. Rapid solidification at the mold wall resulted in fine, equiaxed α-Al grains, enhancing hardness through the Hall-Petch mechanism. Centrifugal segregation added SiO_2 particles to the outer zone, making it more resistant to plastic deformation through the Orowan bowing effect. At 170 °C, the precipitation of coherent and densely distributed θ″ Al_2Cu precipitates was maximum, producing substantial resistance to dislocation motion. These combined effects explain the peak hardness of 138.96 BHN in this segment, which is consistent with patterns observed for similar Al-Mg-Si and Al-Si-Mg-Cu alloys [20–22]. The outer region's rapid cooling results in fine, equiaxed α-Al grains and a refined, uniform distribution of secondary phases, enhancing mechanical properties [23,24].

The middle segment exhibited hardness values slightly lower than the outer segment but still significantly higher than the inner segment, typically ranging from 110–125 BHN depending on aging temperature. This is consistent with its intermediate microstructure, where α-Al grains are moderately refined and the distribution of SiO_2 particles and Al_2Cu precipitates remains balanced. Although the density of precipitates is lower than that of the outer zone, the middle segment retains considerable precipitation strengthening at 170 °C, producing hardness values above 120 BHN during peak aging [11,25].

The inner segment consistently had the lowest hardness at all aging temperatures, with values around 90 BHN at 140 °C, indicating that the material was under-aged and still dominated

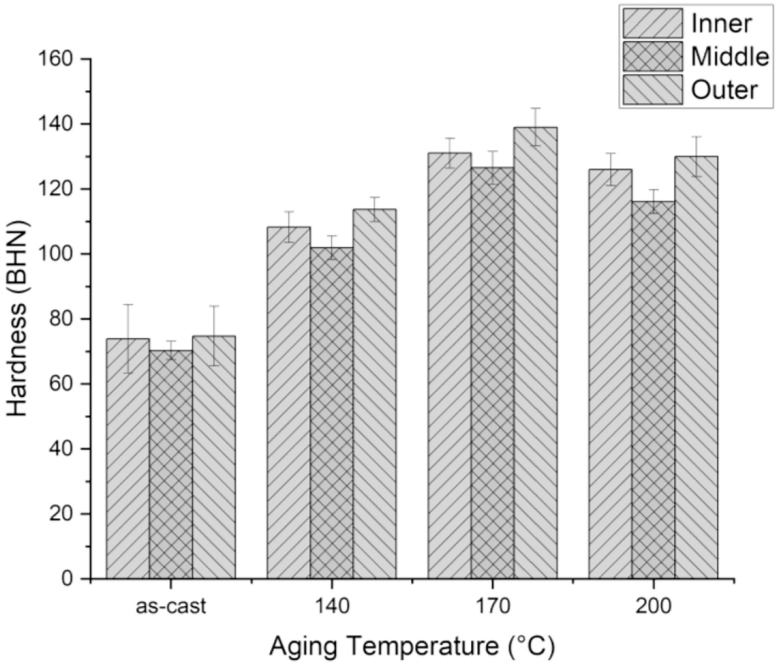

Figure 6. Hardness of inner, middle and outer segment of composites with artificial aging treatment

by GP zones and early-stage nuclei, which provided limited strengthening. The slow cooling rate in this location resulted in coarse dendritic α-Al grains and kept the acicular morphology of eutectic β-Si, leading to lower hardness [26]. The limited segregation of SiO_2 into the inner region additionally decreases the contribution of particle strengthening. These characteristics explain the continued softness of the inner zone even as aging temperatures rise to 170 °C and 200 °C.

The effect of aging temperature strengthens the microstructural interpretation. At 140 ºC, all sections showed reduced hardness due to insufficient solute diffusion to create a large density of strengthening θ″ precipitates. This is consistent with recent research suggesting that aging below 160 °C inhibits precipitation hardening [19]. At 170 °C, the composite reached peak aging, providing the maximum hardness across all zones, particularly the outer region with 138.96 BHN, which is consistent with the behavior observed in Al-Si-Mg-Cu alloys [20–22]. Increasing the aging temperature to 200 °C led to over-aging, reflected in a clear reduction in hardness in every segment. This decrease results from precipitate coarsening, as θ″ transforms into θ′ and partially into equilibrium θ, reducing coherency and weakening their ability to impede dislocations.

Overall, the hardness response is strongly correlated with microstructural evolution. Fine α-Al grains, abundant θ″ precipitates, and high SiO_2 particle concentrations in the outer region produce the highest hardness, while the coarse dendritic microstructure and limited precipitation in the inner region explain its consistently low hardness values. The quantitative hardness differences among the segments outer at 138.96 BHN, middle around 120 BHN, and inner around 90 BHN are therefore fully consistent with the metallographic findings and the standard progression of precipitation hardening from under-aging to peak aging, and finally over-aging.

IMPACT TEST RESULTS

The impact toughness results show a distinct pattern across the radial sections of the centrifugal casting, with the middle region consistently exhibiting the highest toughness, and the maximum value occurring at the highest artificial aging temperature of 200 °C (Figure 7). In the middle region, cooling rate during solidification is moderate, resulting in an intermediate α-Al grain size that is neither too fine nor too coarse. This balanced grain structure offers the best strength-to-ductility ratio possible. At 200 °C, the alloy's Al_2Cu precipitates have coarsened enough to minimize matrix hardening without serious embrittlement. At this elevated aging temperature, the eutectic β-Si undergoes additional spheroidization, lowering its angularity and

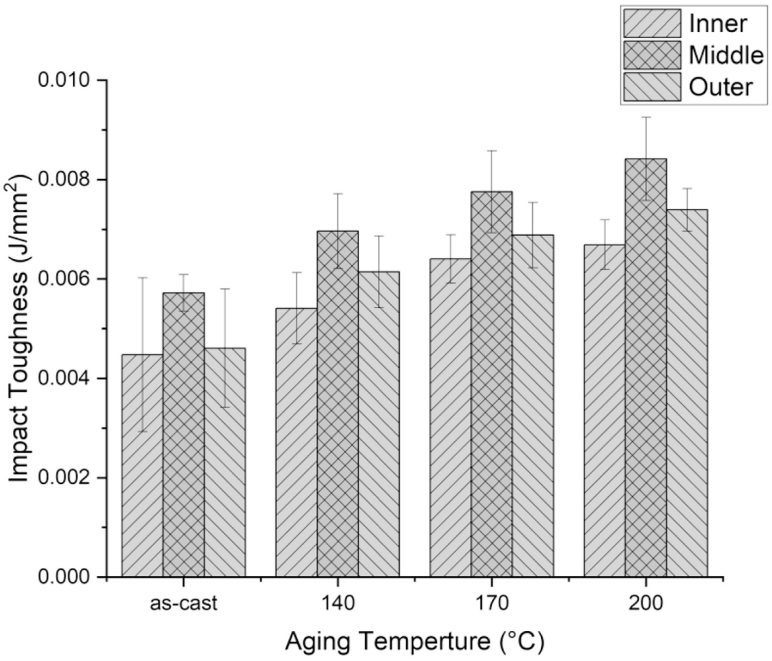

Figure 7. Toughness of inner, middle and outer segment of composites with artificial aging treatment

ability to initiate cracks [27]. The resulting microstructure promotes enhanced plastic deformation during impact, explaining why the middle region exhibits peak toughness at 200 °C.

The outside segment, with refined α-Al grains and high SiO_2 particle concentration, has lower toughness than the intermediate region. This is because the outer zone is inherent harder and less flexible as a result of rapid cooling and thick precipitation during aging. The inner region consistently has the lowest impact toughness at all temperatures. Slow cooling during solidification produces coarse dendritic α-Al grains, together with acicular β-Si that remains sharp and unrefined, acting as stress concentrators. These features provide easy paths for crack initiation and propagation, resulting in limited energy absorption during impact loading [28]. At 200 °C, the coarsening of precipitates reduces hardness but does not significantly restore ductility because the high reinforcement concentration continues to restrict plastic flow. The effect of aging temperature is obvious in the fracture properties of all radial zones. At 140 °C, under-aging leads to insufficient precipitation strengthening and limited spheroidization, resulting in brittle, planar fracture surfaces and low toughness. At 170 °C, toughness improves, particularly in the middle and outer regions, as θ″ precipitates strengthen the matrix and β-Si particles begin to round [20]. However, the most significant increase in toughness occurs at 200 °C, when the composite enters a partially over-aged state that improves ductility without significantly reducing strength. This is especially advantageous for the middle region, which has a balanced microstructure and can fully exploit these changes [21].

FRACTOGRAPHY

This phenomenon can be fully explained by the observed microstructural conditions and fracture characteristics as seen in Figure 8. The center region has more evenly distributed SiO_2 particles and Al_2Cu precipitates compared to the other two zones. There is no clumping or agglomeration, which is a common cause of stress concentration. Because of the absence of agglomeration, cracks cannot form directly at a single weak site and must instead move via a more uniform microstructural. This process naturally increases the energy required for crack propagation. Under the 200 °C aging condition, which produces the highest impact value, the middle region microstructure exhibits a balance between strength and deformability. The produced Al_2Cu precipitates have undergone more stable development, limiting excessive hardening and increasing brittleness. The β-Si morphology has more significant spheroidization, which prevents sharp edges that might cause cracks. This combination results in an aluminum matrix that is both robust and capable of plastic deformation under impact stresses. These characteristic are mirrored on the fracture surface. Despite being examined through an optical microscope, the fracture surface of the middle section seems rougher, less flat, and has a tortuous fracture course. These characteristics imply that the material experienced more substantial plastic deformation prior to failure. The crack does not propagate in a straight line like brittle fracture, but is periodically deflected by the reinforcing particles and precipitates in the matrix. Each crack deflection consumes additional energy, resulting in a higher total energy required to fracture the specimen. Meanwhile, the outer region exhibits moderate toughness because, despite its finer grains, the higher concentration of particles and precipitates results in a harder matrix that is less capable of plastic deformation. The inner region exhibits the lowest toughness due to coarser grains, acicular β-Si, and non-uniform particle distribution, which allow cracks to develop more rapidly and more linearly.

SEM observations of the impact fracture surfaces exhibit a similar tendency, indicating a mixed-mode fracture mechanism involving both ductile and brittle features. The fracture surfaces are generally rough and tortuous, suggesting that localized plastic deformation occurred in the aluminum matrix prior to final failure, which prevented straight crack propagation. In some regions, relatively smooth and flat areas are also observed, reflecting localized brittle fracture, particularly at crack initiation sites. The coexistence of these features confirms that failure is governed by a combined effect of matrix plasticity and deformation constraints imposed by the reinforcement particles. EDS analysis reveals that aluminum and silicon are the dominant elements on the fracture surfaces, originating from the Al–Si matrix and silicon-based oxide particles (Figure 9). The relatively uniform distribution of Si indicates a homogeneous dispersion of these particles, which actively participate in the fracture process by

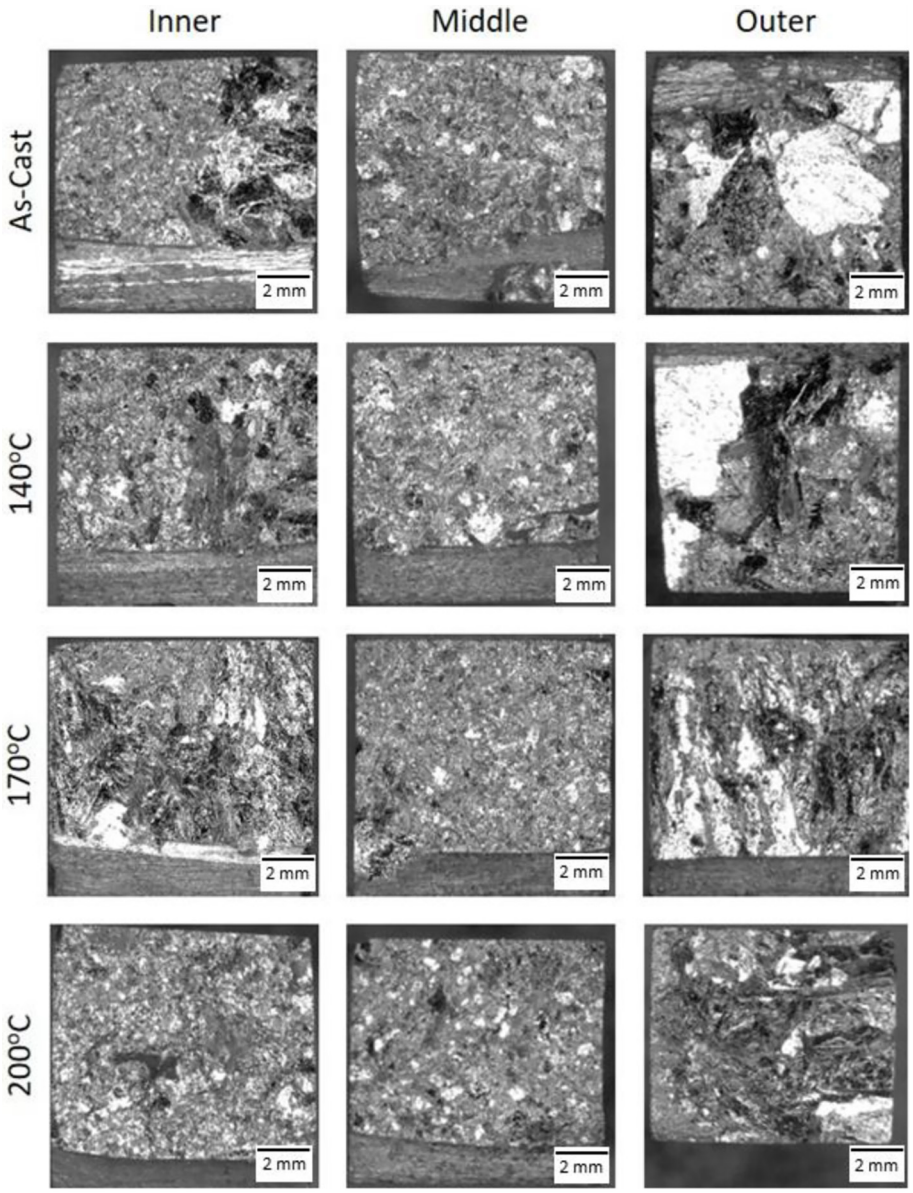

Figure 8. Fracture surfaces of impact test

deflecting and branching cracks, thereby increasing the energy required for crack propagation. The absence of significant elemental segregation further suggests that fracture behavior is primarily controlled by matrix–particle interactions rather than by localized chemical inhomogeneity.

DISCUSSION

A thorough examination of the metallographic results, hardness tests, impact tests, and XRD characterizations reveals that the mechanical behavior of Al-Si-Cu composites produced by the vertical centrifugal casting process is heavily influenced by phase evolution during solidification and artificial aging. This material's strengthening mechanism combines reinforcing precipitates, eutectic particle morphological changes, SiO_2 reinforcement distribution, and local microstructural interactions to limit fracture propagation. These findings illustrate the fundamental trade-off between hardness and toughness as a function of artificial aging temperature. The peak-aged condition at 170 °C optimized hardness through fine precipitation strengthening but reduced toughness, while the over-aged condition at 200 °C enhanced toughness at the expense of strength. Similar trends have been reported in Al–Si–Cu alloys under T6 treatment, where θ″ precipitates dominate peak hardness and coarsened θ′/θ phases promote ductility [29,30]. The findings emphasize the need

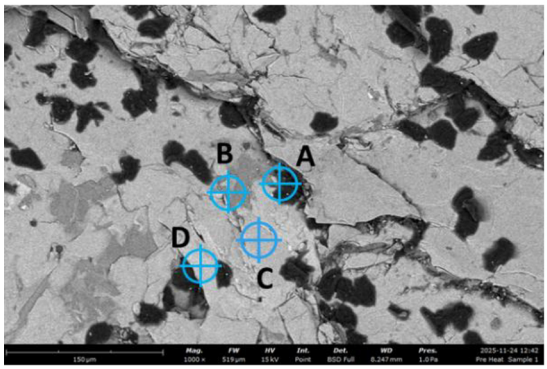

	Element Number	Element Symbol	Element Name	Atomic Conc.	Weight Conc.
A	6	C	Carbon	79.548	64.635
	8	O	Oxygen	7.752	8.392
	11	Na	Sodium	0.193	0.300
	13	Al	Aluminum	8.596	15.684
	14	Si	Silicon	1.419	2.697
	16	S	Sulfur	0.414	0.899
	17	Cl	Chlorine	0.333	0.799
	26	Fe	Iron	1.745	6.593
B	6	C	Carbon	53.805	33.433
	8	O	Oxygen	1.330	1.101
	11	Na	Sodium	0.000	0.000
	13	Al	Aluminum	1.506	2.102
	14	Si	Silicon	43.116	62.663
	17	Cl	Chlorine	0.000	0.000
	26	Fe	Iron	0.242	0.701
C	6	C	Carbon	21.324	9.300
	8	O	Oxygen	0.861	0.500
	11	Na	Sodium	0.000	0.000
	13	Al	Aluminum	56.873	55.700
	14	Si	Silicon	8.137	8.300
	17	Cl	Chlorine	0.078	0.100
	26	Fe	Iron	9.960	20.200
	28	Ni	Nickel	2.768	5.900
D	6	C	Carbon	26.503	11.800
	8	O	Oxygen	1.686	1.000
	11	Na	Sodium	0.000	0.000
	13	Al	Aluminum	56.810	56.800
	14	Si	Silicon	1.440	1.500
	17	Cl	Chlorine	0.076	0.100
	26	Fe	Iron	5.120	10.600
	28	Ni	Nickel	8.365	18.200

Figure 9. SEM EDS results of fracture aging temperature 200 °C in middle segment

to adjusting artificial aging parameters depending on the targeted mechanical properties. Aging at 170 °C is optimal for maximum hardness and wear resistance, whereas 200 °C provides superior impact toughness and fracture resistance. In the 200 °C aging heat treatment, the distribution of Al_2Cu precipitates after aging appears more even, not concentrated as large clusters when compared to conditions without heat treatment as seen in. This homogeneous distribution indicates that the heat treatment process successfully breaks down the Cu segregation that previously appeared in the as-cast condition. Even distribution of Al_2Cu improves mechanical properties by inhibiting dislocation movement (precipitation hardening), creating a complex crack propagation path, and increasing material strength and toughness. The main strengthening mechanisms are precipitation hardening, Orowan strengthening from dislocation interactions with SiO_2 particles and Al_2Cu precipitates, and load transfer from the matrix to reinforcement particles. Crack deflection, bridging, and β-Si spheroidization improve toughness, particularly in the middle area, after 200 °C aging. The balance between hardness and toughness in this region is considered optimal because the precipitates have grown to a size sufficient to inhibit dislocations, but not cause embrittlement. It should be noted that this study has several limitations that may influence the interpretation of the results. The size and number density of precipitates were not quantitatively measured, and the precipitation behavior was primarily inferred from microstructural trends and mechanical responses. Although these properties are highly relevant for functionally graded materials subjected to wear and impact loading, the absence of tensile and fatigue testing limits the assessment of structural performance under service-like conditions. Future work incorporating tensile, fatigue, and wear tests would further clarify the applicability of these materials for automotive and aerospace components. Despite these limitations, the observed trends are consistent and provide meaningful insights into the interaction between microstructural gradients and mechanical behavior in centrifugally cast recycled aluminum composites.

CONCLUSIONS

This study demonstrated the combined influence of centrifugal casting and artificial aging temperature on the microstructural evolution and

mechanical performance of re-melted aluminum piston alloys reinforced with Cu and SiO_2. The centrifugal casting process produced distinct phase distributions across the outer, middle, and inner segments due to differences in cooling rate and particle segregation. Artificial aging temperature further controlled the morphology and effectiveness of strengthening phases. The peak-aged condition at 170 °C yielded the highest hardness (138.96 BHN) in the outer segment, attributed to refined α-Al grains, globular β-Si particles, and coherent θ″ Al_2Cu precipitates that enhanced precipitation hardening. In contrast, the over-aged condition at 200 °C promoted extensive β-Si spheroidization and precipitate coarsening, which reduced hardness but significantly improved toughness, particularly in the inner segment. The middle segment consistently showed a balance of hardness and toughness, reflecting its intermediate microstructure. This findings confirm a trade-off between hardness and toughness governed by artificial aging. For applications requiring maximum wear resistance and strength, an aging temperature of 170 °C is optimal, whereas 200 °C provides superior impact toughness and fracture resistance. These results highlight the importance of tailoring artificial aging treatments to achieve application-specific performance in recycled Al–Si–Cu piston alloys.

Acknowledgment

The authors would like to express their gratitude to Universitas Sebelas Maret for providing various facilities and financial support through the PKGR-UNS 2025 research schema with contract no. 371/UN27.22/PT.01.03/2025.

REFERENCES

1. Bintoro SR, Putri EDWS, Suhartono A, Muhayat N, Badaruddin M, Fauzun, Triyono. Effect of welding environment on fatigue crack growth rate of aluminium alloy 1100. J Achiev Mater Manuf Eng 2024;122:49–60. https://doi.org/10.5604/01.3001.0054.4848
2. Georgantzia E, Gkantou M, Kamaris GS. Aluminium alloys as structural material: A review of research. Eng Struct 2021;227:111372. https://doi.org/https://doi.org/10.1016/j.engstruct.2020.111372
3. Lutiyatmi, Surojo E, Muhayat N, Azka M, Triyono. The effect of weight fraction on the microstructure and mechanical properties of aluminum–cast iron slag composites. Eng Technol Appl Sci Res 2025;15:24715–22. https://doi.org/10.48084/etasr.10943
4. Al-Alimi S, Yusuf NK, Ghaleb AM, Lajis MA, Shamsudin S, Zhou W, Altharan YM, Abdulwahab HS, Saif Y, Didane DH, S T T I, Adam A. Recycling aluminium for sustainable development: A review of different processing technologies in green manufacturing. Results Eng 2024;23:102566. https://doi.org/10.1016/j.rineng.2024.102566
5. Kim M, Kim K Il, Lee JK, Hyun SK, Kim KT. Effect of GBF Process conditions on the microstructural characteristic, melt quality and mechanical properties of Al-Si alloys with scrap addition. Materials (Basel) 2025;18:1–14. https://doi.org/10.3390/ma18050943
6. Shower P, Morris JR, Shin D, Radhakrishnan B, Allard LF, Shyam A. Temperature-dependent stability of θ′-Al2Cu precipitates investigated with phase field simulations and experiments. Materialia 2019;5:100185. https://doi.org/10.1016/j.mtla.2018.100185
7. Wang Z, Chen J, Liu B, Pan R, Gao Y, Li Y. Effect of deep cryogenic treatment on the artificial ageing behavior of SiCp–AA2009 composite. Metals (Basel) 2022;12:1–14. https://doi.org/10.3390/met12101767
8. Matejka M, Bolibruchová D, Sýkorová M. Effect of Ti addition on the hot-tearing susceptibility of the AlSi5Cu2Mg alloy. Metals (Basel) 2024;14. https://doi.org/10.3390/met14060703
9. Bintoro SR, Surojo E, Muhayat N, Triyono. A comprehensive review on fusion arc welding of aluminum matrix composites: challenges, mechanisms, and advancements. Results Eng 2025;27:106257. https://doi.org/10.1016/j.rineng.2025.106257
10. Kadam MS, Shinde VD. Stir cast aluminium metal matrix composites with mechanical and micro-structural behavior: A review. Mater Today Proc 2020;27:845–52. https://doi.org/10.1016/j.matpr.2020.01.017
11. Verma RK, Parganiha D, Chopkar M. A review on fabrication and characteristics of functionally graded aluminum matrix composites fabricated by centrifugal casting method. SN Appl Sci 2021;3. https://doi.org/10.1007/s42452-021-04200-8
12. Miclosina CO, Belu-Nica R, Ciubotariu CR, Marginean G. Processing and evaluation of an aluminum matrix composite material. J Compos Sci 2025;9:1–12. https://doi.org/10.3390/jcs9070335
13. Kareem A, Qudeiri JA, Abdudeen A, Ahammed T, Ziout A. A review on aa 6061 metal matrix composites produced by stir casting. Materials (Basel) 2021;14:1–22. https://doi.org/10.3390/ma14010175
14. Zhang X, Chen T. Simultaneously enhancing the strength and ductility of particulate-reinforced aluminum matrix composite by aging treatment. J Mater Res 2021;36:3445–59. https://doi.org/10.1557/s43578-021-00389-x

15. Setyawan H, Muhayat N, Yuliadi MZ, Manurung YHP, Triyono. Effect of artificial ageing temperature in T6-heat treatment on the mechanical properties of dissimilar metals weld between AA5083 and AA6063 2023;123:72–85. https://doi.org/10.5604/01.3001.0054.2494
16. Wiengmoon A, Apichai P, Pearce JTH, Chairuangsri T. Effects of T6 age hardening on microstructure and mechanical properties of Al-Si-Cu cast aluminium alloy. Adv Mater Res 2013;770:88–91. https://doi.org/10.4028/www.scientific.net/AMR.770.88
17. Deng Y, Huang G, Cao L, Wu X, Huang L. Effect of ageing temperature on precipitation of Al-Cu-Li-Mn-Zr alloy. J Cent South Univ 2018;25:1340–9. https://doi.org/10.1007/s11771-018-3830-8
18. Wei W, Zuo R, Xue D, Wen S, Wu Y, Shi W, Zhou X, Huang H, Wu X, Gao K, Rong L, Nie Z. Effect of aging treatment on the precipitation behavior of a novel Al-Cu-Zr Cast alloy. Materials (Basel) 2022;15. https://doi.org/10.3390/ma15228163
19. Zamani M, Toschi S, Morri A, Ceschini L, Seifeddine S. Optimisation of heat treatment of Al–Cu–(Mg–Ag) cast alloys. J Therm Anal Calorim 2020;139:3427–40. https://doi.org/10.1007/s10973-019-08702-x
20. Sjölander E, Seifeddine S. Artificial ageing of Al–Si–Cu–Mg casting alloys. Mater Sci Eng A 2011;528:7402–9. https://doi.org/10.1016/j.msea.2011.06.036
21. Ren J, Hong Z, Zhou Q, Xu X, Yin S. Effect of aging treatment temperature on microstructure and properties of Al-Si-Mg cast aluminum alloy. J Mater Eng Perform 2024;33:13284–92. https://doi.org/10.1007/s11665-023-08911-4
22. Sjölander E, Seifeddine S. The heat treatment of Al–Si–Cu–Mg casting alloys. J Mater Process Technol 2010;210:1249–59. https://doi.org/10.1016/j.jmatprotec.2010.03.020
23. Ram SC, Chattopadhyay K, Gupta D, Bhushan A, Moray A, Kaushik S, Saha S. Mechanical properties, dry sliding wear resistance, and microstructural characterization of in-situ Al-17Si-Al_3Zr/Al_2O_3 FG-composite synthesized via vertical centrifugal casting technique. Compos Interfaces 2025;32:297–319. https://doi.org/10.1080/09276440.2024.2417159
24. Ambigai R, Prabhu S. Characterization and mechanical analysis of functionally graded Al-Si3N4 composites through centrifugal process. J Mater Eng Perform 2021;30:7328–42. https://doi.org/10.1007/s11665-021-05963-2
25. Radhika N, Jojith R, Vignesh S, Raghavenderen HS, Abinav S, Adediran AA. Characterization, mechanical properties, and wear behavior of functionally graded aluminum hybrid composite. Sci Rep 2024;14:1–17. https://doi.org/10.1038/s41598-024-70189-w
26. Wang K, Zhang ZM, Yu T, He NJ, Zhu ZZ. The transfer behavior in centrifugal casting of SiCp/Al composites. J Mater Process Technol 2017;242:60–7. https://doi.org/10.1016/j.jmatprotec.2016.11.019
27. Li X, Hong Y, Wang Z-W, Lin N, Liu J-L, Nie Q. Effect of heat treatment on the microstructure and mechanical properties of Al-Si-Cu-Mg Aluminum Alloy Reinforced with SiC Particles. Metals (Basel) 2019;9:11–9. https://doi.org/doi:10.3390/met9111205
28. Adelakin TK, Suárez OM. Study of boride-reinforced aluminum matrix composites produced via centrifugal casting. Mater Manuf Process 2011;26:338–45. https://doi.org/10.1080/10426910903124829
29. Fabrizi A, Capuzzi S, De Mori A, Timelli G. Effect of T6 heat treatment on the microstructure and hardness of secondary AlSi9Cu3(Fe) alloys produced by semi-solid SEED process. Metals (Basel) 2018;8. https://doi.org/10.3390/met8100750
30. Dong X, Amirkhanlou S, Ji S. Formation of strength platform in cast Al–Si–Mg–Cu alloys. Sci Rep 2019;9:1–11. https://doi.org/10.1038/s41598-019-46134-7